J. Nonlinear Sci. Vol. 14: pp. 383–404 (2004)
DOI: 10.1007/s00332-004-0616-y

Journal of
Nonlinear
Science



# Chaos and Period-Adding: Experimental and Numerical Verification of the Grazing Bifurcation

P. T. Piiroinen,[†] L. N. Virgin,[‡] and A. R. Champneys[†]

[†] Bristol Center for Applied Nonlinear Mathematics, Department of Engineering Mathematics, University of Bristol, Bristol BS8 1TR, United Kingdom

[‡] Department of Mechanical Engineering, Duke University, Durham, NC 27708-0300, USA

Received November 20, 2003; accepted May 12, 2004
Online publication July 26, 2004
Communicated by S. Strogatz

**Summary.** Experimental results are presented for a single-degree-of-freedom horizontally excited pendulum that is allowed to impact with a rigid stop at a fixed angle $\hat{\theta}$ to the vertical. By inclining the apparatus, the pendulum is allowed to swing in an effectively reduced gravity, so that for each fixed $\hat{\theta}$ less than a critical value, a forcing frequency is found such that a period-one limit cycle motion just grazes with the stop. Experimental measurements show the immediate onset of chaotic dynamics and a period-adding cascade for slightly higher frequencies. These results are compared with a numerical simulation and continuation of solutions to a mathematical model of the system, which shows the same qualitative effects. From the model, the theory of discontinuity mappings due to Nordmark is applied to derive the coefficients of the square-root normal form map of the grazing bifurcation for this system. The grazing periodic orbit and its linearisation are found using a numerical continuation method for hybrid systems. From this, the normal-form coefficients are computed, which in this case imply that a jump to chaos and period-adding cascade occurs. Excellent quantitative agreement is found between the model simulation and the map, even over wide parameter ranges. Qualitatively, both accurately predict the experimental results, and after a slight change in the effective damping value, a striking quantitative agreement is found too.

## 1. Introduction

Many mechanical systems exhibiting sustained finite-amplitude oscillatory motion do so because of some kind of discontinuity or nonsmoothness. Effects of this nature include vibro-impact, rattling due to freeplay or backlash, stick-slip motion due to friction as well as the discrete or delayed interaction with a control system; see for example [50], [5], [44], [3], [2], [17], to name but a few of the vast number of references on this subject.

There are also analogues in electronics (e.g. [11]), biology (e.g. [30]), and almost all other areas in which dynamical systems arise. Such systems have been found to show a remarkable variety of different long-time behaviour, such as periodic, quasi-periodic, and chaotic motions, and to undergo all the bifurcations that may occur for smooth systems (fold, Hopf, period-doubling, etc.). They also undergo bifurcations that are unique to nonsmooth systems (so-called $C$-bifurcations [16], [14]), which occur when an $\omega$-limit set approaches a discontinuity surface within the phase space. Such transitions include border-collision bifurcation in maps [16], [38], boundary transition of equilibria in flows [31], [30], or the grazing [35], [9], sliding [15], chattering [6], or corner-collision [13] of a periodic orbit. In this paper we shall focus on the bifurcation caused by *grazing* (zero-velocity impact) of a periodic orbit with a hard constraint.

There are basically two different ways to model impacts in mechanics (see e.g. [48], [42], [55]): either as elastic, with the contact between the bodies taking a finite time, or as completely rigid and instantaneous. In the former case there is a small penetration into the unilateral stop and typically the propagation of shock waves, while in the latter, one assumes that the velocity is immediately reversed at impact with some impulsive loss of energy (a restitution law). We shall adopt the second approach here, which has been shown to be a good model for point contacts in the absence of friction. Hence one typically arrives at low-degree-of-freedom smooth (even linear) dynamical models between impacts, with a discontinuity in velocity whenever the system hits some hard constraint in configuration space. Practical examples of such impact-oscillator systems include bouncing balls [22], rattling gears [26], colliding boiler tubes [21], car suspensions [25], Braille printers [24], [10], and percussive drilling [28], [23].

It has been known since the pioneering work of Peterka [40], [41], who studied a simple harmonic oscillator with sinusoidal forcing and impact, that low velocity impact can have a profound implication for the dynamics. Shaw and Holmes [45] showed that such grazing events in impact oscillators can lead to the disappearance of stable periodic motion, and Whiston [53], [52] showed the onset of chaotic motions of low velocity impacts which can have a characteristic *fingered* appearance (see also Thompson and Ghaffari [49] and Figure 11 below). The key idea is that Poincaré maps associated with grazing have infinite local stretching due to a square-root singularity, which has strong implications on the geometry of phase space [54], [7].

As with smooth dynamical systems, in order to explain this and related behaviour, it is desirable to derive *normal forms* that enable all possible long-term dynamics at nearby parameter values to be described. The same philosophy applies to nonsmooth bifurcations such as that brought about by grazing. The key concept here is that of the *discontinuity mapping* introduced by Nordmark [35], [36], [18]. This allows the analytical derivation of the appropriate Poincaré map directly from the flow, given only information about the grazing periodic orbit and its linearisation (see Section 5). The resulting mappings have a square-root singularity, and their dynamics can be classified using simple iterative techniques [8], [37]. Depending on the coefficients of the normal form, various scenarios are possible. These include the sudden birth or destruction of stable periodic motion, the sudden jump to chaos (with fingered attractors), and so called *period-adding*, where an infinite number of periodic orbits appear that become stable in successive parameter intervals with the periodicity increased (decreased) by one each time. These intervals may occur as *windows* interspersed within the main region of chaos, and should be

contrasted with the situation for smooth unimodal maps where the periodicity of the windows obeys the usual Sarkovskii ordering [12].

There is significant experimental evidence for complex dynamics in impact oscillator systems. See for example [4], [47], [20], [51]. Some of the most convincing experimental verification of the dynamics of a single-degree-of-freedom impact oscillator occurs in the work of Oestreich et al. [39], where excellent agreement is found between experimental and numerical one-parameter bifurcation diagrams. Within the parameter sweep are values where already impacting orbits undergo further (internal) grazing with the stop. However we are not aware of any work on experimental verification of a grazing bifurcation where the pregrazing orbit is a period-one nonimpacting limit cycle. It is precisely this situation we investigate here, and in addition to comparison with numerics, we shall also evaluate the normal form for the grazing to explain the details of the dynamics observed in the experiment. In so doing we shall find a close match of both the experiments and the numerics not just for the existence of grazing but also in the details of the ensuing dynamics described by the normal form theory.

The rest of this paper is organized as follows. In Section 2 the experimental set-up is introduced and its results are presented. Section 3 introduces the equations of motion for the impacting mechanism, and in Section 4 numerical techniques used to simulate and analyze periodic solutions are introduced. In Section 5 some aspects of grazing bifurcation theory are introduced, culminating in the derivation of the discontinuity map for the specific problem analysed here. Section 6 presents results of the numerics and analysis and compares them with the experiment, including a brief discussion on overcoming experimental uncertainty. Finally, Section 7 draws conclusions.

## 2. Experiments

The experimental results described here were obtained using the apparatus employed in the earlier results of Bayly, Virgin, and Slade [4], [46]. Those works focused on chattering solutions and the extraction of data from recording of the time between impacts. Here, a novel adaptation of the apparatus is considered which allows the variation of the position of the impacting stop in order to specifically investigate grazing.

### *2.1. The Experimental System*

A simple rigid-arm pendulum that strikes a vertical impact surface is an easily realized single-degree-of-freedom discontinuous mechanical oscillator [4]. By horizontally shaking the supporting pivot of the pendulum, we can observe a variety of dynamic behavior, including chaos. However, with the impact barrier located at static equilibrium, the velocity of impact tends to be relatively high and thus grazing bifurcations of the fundamental *period-one* (i.e., with the same period as the forcing) do not typically occur. But, by inclining the angle at which the pendulum mass strikes the barrier, it is possible to observe the subtle transition between noncontacting and contacting dynamic behavior (see Figure 1). If the impact surface is placed sufficiently far from static equilibrium (i.e., to the left of equilibrium) and the forcing is relatively low, then impact will not take place. For intermediate angles of impact, as a parameter is changed, however, contact is

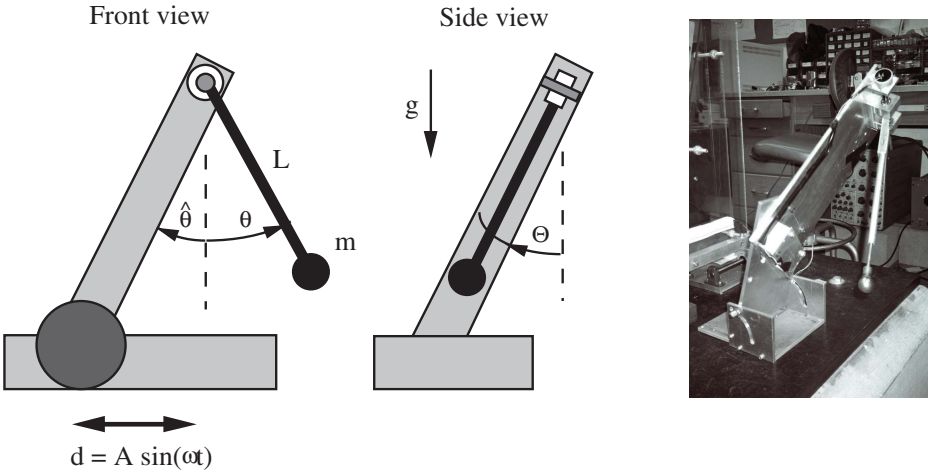


**Fig. 1.** Schematic (left and middle) and photo (right) of the pendulum/impact barrier assembly.

initiated, and it is the interesting behavior associated with this discrete transition that is the focus of the current study.

The pendulum is constructed using a relatively light aluminium arm of length 305 mm and a steel mass of diameter 25.4 mm attached at the end. The pivot of the pendulum consists of low-friction bearings, and a rotational potentiometer measures the angle $\theta(t)$. The assembly is mounted on a Scotch-yoke driven shake table which imparts a harmonic base displacement. Due to speed limitations of the forcing mechanism, the assembly was inclined at an angle of $\Theta = 1.33$ radians (out of plane; see the right-hand side of Figure 1) in order to change the effect of gravity, i.e., $g_e = 0.24g$, and thus reduce the natural frequency of the system. The measured natural frequency indicated that the pendulum arm and end mass resulted in an effective length of an ideal pendulum of $L = 225$ mm. The forcing amplitude $A$ was chosen as 50.8 mm (centre to peak) and this was held fixed for all the experiments. The angle of contact with the impact barrier $\hat{\theta}$ and the forcing frequency $\omega$ were used as the primary control parameters: the former fixed at discrete values at intervals of $10^\circ$ and the latter varied statically by small amounts. The forcing mechanism allowed a discrete (Poincaré) sampling of the response, i.e., every time the flywheel of the Scotch-yoke passed through a certain phase, the angle of the pendulum $\theta$ at that specific instant of time was extracted. At each new parameter value data was recorded, with a rotational potentiometer attached to the pivot of the pendulum, only after a sufficient amount of time for transients to decay.

A crucial issue in modelling many mechanical systems is the estimation of the amount of damping. Damping in this system is primarily due to the coefficient of restitution at impact, but may also arise from a number of other factors, such as coulomb friction in the bearing and viscous air drag. In order to estimate the overall damping, a simple logarithmic decrement method was used on the measured response when $\hat{\theta} = 0$ and no forcing was present. Successive peak amplitudes $A_k$, $k = 1, 2, \ldots$, were recorded and

an overall damping factor $D$ recorded according to the standard formula

$$D = \frac{1}{4\pi \hat{k}} \ln\left(\frac{A_k}{A_{k+\hat{k}}}\right), \tag{1}$$

where $\hat{k}$ is a positive integer. The effect of external noise may be minimized by choosing amplitudes a number of impacts apart, i.e., by choosing $\hat{k} > 1$. A value for $D$ was obtained by averaging over several runs, from which it was estimated that $D = 0.07$, i.e., 7% of critical damping. It is notable that this damping ratio includes impact losses, as will be discussed further in Section 3.

### *2.2. Results*

Figures 2 and 3 summarize, for four different values of $\hat{\theta}$, the response of the pendulum when the forcing frequency is gradually increased through the range of primary resonance. Forcing frequency is measured as a ratio $\eta$ to the natural frequency of an impacting pendulum (see (3) below), so that the primary resonance is at $\eta = 1/2$.

The angle of the stop was varied in intervals of $10^\circ$ from $\hat{\theta} = 0^\circ$. The case $\hat{\theta} = 0^\circ$ was thoroughly described in [4]. Complex dynamics occurs, but grazing bifurcations do not play a major role, so we do not consider this case further here. For each $\hat{\theta}$-value between $10^\circ$ and $40^\circ$ inclusive, a critical forcing frequency $\eta = \eta_c$ was found below which a period-one limit cycle exists that does not impact. At $\eta_c$ this limit cycle just grazes with the stop, and impacting motion is found for $\eta > \eta_c$, at first a complex sequence of chaotic and periodic motion, until eventually for large-enough $\eta$ the motion settles into a period-one motion that impacts precisely once per period. For $\hat{\theta} = 50^\circ$ it was found that the pendulum amplitude is always less than the barrier angle $\theta(t) < \hat{\theta}$ for the forcing amplitude $A = 50.8$ mm, and hence no impacting motion takes place. We do not present results for this case.

Consider now the details of the four cases $\hat{\theta} = 10^\circ, 20^\circ, 30^\circ, 40^\circ$ presented in panels (a)–(d) of Figure 2. Note first that the frequency value of the grazing bifurcation $\eta_c$ increases with $\hat{\theta}$.

At $\hat{\theta} = 10^\circ$, $\eta_c \approx 0.343$, at which value there is a sudden jump to impacting chaotic behaviour. Time-series data extracted from the dynamics are shown in Figure 3(a), where the high-frequency effects were filtered out both within the hardware and using the Butterworth algorithm within the LabVIEW software. However, the experiment exhibited very high signal-to-noise ratios and hence filtering had a relatively minor effect in any event. From this figure we note the quality of the data due to the high precision (single-turn) rotational potentiometer interfaced with LabVIEW. The continuous measurement of the angle was also independently verified using discrete measurements of the impact events (see [46]). A phase space reconstruction of this dynamics, using Takens's method of delays (with a delay of one quarter of a cycle) is shown in Figure 3(b). This shows the characteristic shape of a strange attractor. At higher $\eta$ ($0.35 < \eta < 0.36$) a significant window of *period-two* periodic motion is observed, culminating in a reverse supercritical period-doubling bifurcation to period-one impacting motion.

For $\hat{\theta} = 20^\circ$, $\eta_c$ is approximately 0.405, and after a brief interval of apparently chaotic behaviour, there is a significant $\eta$-window ($0.406 < \eta < 0.42$) of *period-three*

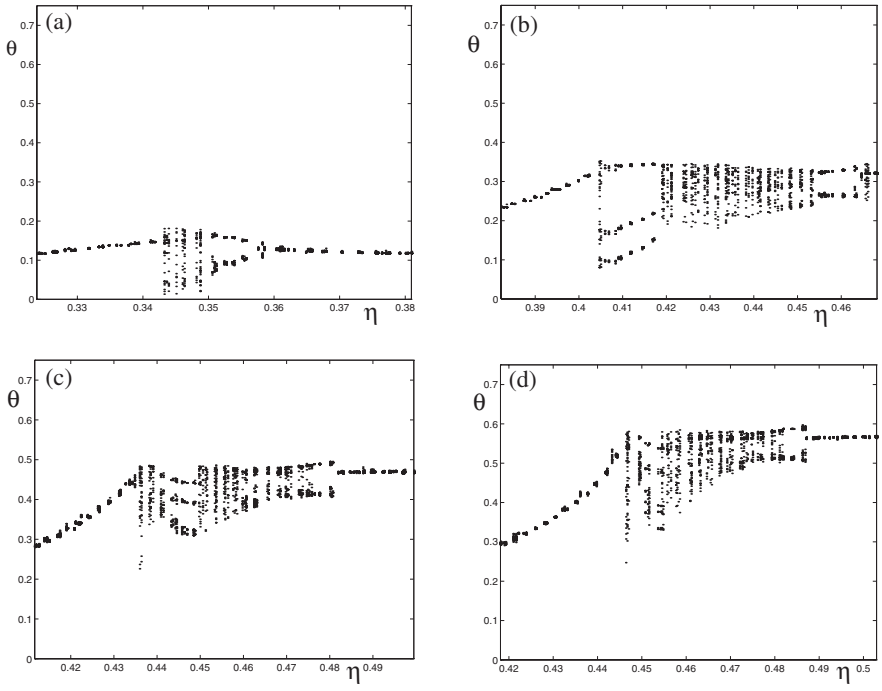


**Fig. 2.** Experimental bifurcation diagrams in which the response is sampled once during a forcing cycle (at an arbitrary but consistent phase $p$). (a) $\hat{\theta} = 10^\circ$, (b) $\hat{\theta} = 20^\circ$, (c) $\hat{\theta} = 30^\circ$, (d) $\hat{\theta} = 40^\circ$.

motion. There then follows a long interval of chaotic behaviour (with possible small periodic windows). This culminates in a window of period-two motion which itself dies in a sudden abrupt jump (possibly through a small interval of chaos) to period-one nonimpacting motion.

For $\hat{\theta} = 30^\circ$, where $\eta_c \approx 0.435$, a pattern appears to be emerging, because after a brief interval of chaos there is a significant window ($0.44 < \eta < 0.45$) of *period-four* impacting motion (whose period was confirmed by looking at the phase-space reconstruction). This is again followed by a long interval of chaos, a period-two window and the eventual jump to the period-one nonimpacting motion.

The case $\hat{\theta} = 40^\circ$, for which $\eta_c \approx 0.446$, completes the pattern. The first significant periodic window (starting around $\eta = 0.45$) contains a *period-five* orbit, which is confirmed by the time series and phase-space reconstruction shown in Figure 3(c),(d). Again there is an interval of chaos, a period-two window and a jump to period-one nonimpacting motion.

In summary, then, the results definitely do not represent what one would expect from the theory of unimodal maps (e.g. [12]) that is replicated in most smooth dynamical systems undergoing period doubling. Here we see a sudden jump to chaos, and as $\hat{\theta}$ is increased, rather than finding a period-doubling cascade, we see a so-called period-adding cascade where the first significant periodic window jumps from period 2, to 3,

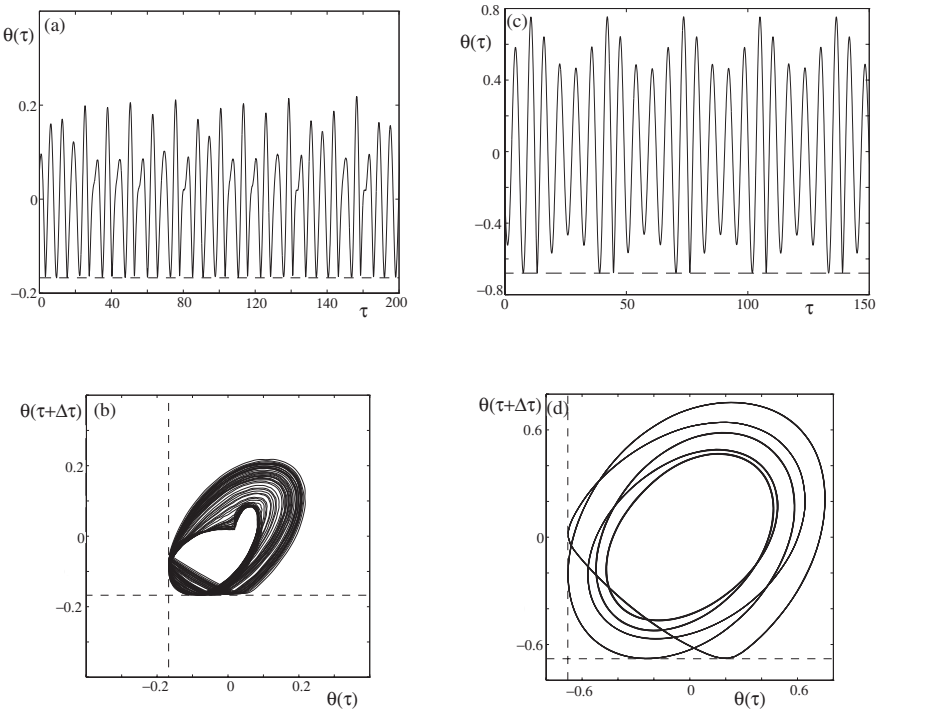


**Fig. 3.** Sample experimental time series and phase projections. (a) and (b) $\hat{\theta} = 10^{\circ}$, $\eta = 0.35$; (c) and (d) $\hat{\theta} = 40^{\circ}$, $\eta = 0.45$.

to 4, to 5. Finally we note that the period-two window is the last to be seen, and (for all cases other than $\hat{\theta} = 10^{\circ}$) this ends abruptly rather than in a reverse supercritical period-doubling.

## 3. Mathematical Model

Equations of motion for a forced, inclined pendulum may be derived using elementary methods,

$$-\frac{\ddot{d}(t)}{L}\cos(\theta) = \ddot{\theta} + \frac{g_e}{L}\sin(\theta) + \kappa\dot{\theta}. \tag{2}$$

Here $d(t) = A\sin(\omega t)$ is the applied support motion, $L$ is the effective length of the pendulum arm, and $g_e$ the effective gravity (cf. Section 2.1). Dissipation is included via a simple linear term $\kappa\dot{\theta}$, as is often assumed, in order to model the various causes of damping (other than the restitution at impact). Following [4], [46], we will nondimensionalize (2) by letting

$$\eta = \frac{\omega}{\omega_0}, \quad \text{where} \qquad \omega_0 = 2\sqrt{\frac{g_e}{L}}, \qquad \tau = \omega t, \qquad \alpha = \frac{A}{L}, \qquad \beta = \frac{\kappa}{2\omega_0}. \tag{3}$$

Here $\omega_0$ is the frequency of small amplitude motion of the impacting oscillator (when $\hat{\theta} = 0$), which is twice the natural frequency of the nonimpacting system. The nondimensionalized equation can then be written as

$$\theta'' + \frac{2\beta}{\eta}\theta' + \frac{1}{4\eta^2}\sin(\theta) = \alpha\cos(\theta)\sin(\tau), \tag{4}$$

where $'$ represents $d/d\tau$. These are then the equations of motion that hold between impacts, i.e., for $\theta < \hat{\theta}$.

At impact $\theta = \hat{\theta}$ we assume a simple restitution law. Let $\tau_{\text{im}}$ be the time at which impact occurs, then we suppose that dimensionless angular velocity is instantaneously reset according to

$$\theta'(\tau_{\text{im}}^+) \leftarrow -r\theta'(\tau_{\text{im}}^-), \quad 0 \le r \le 1, \tag{5}$$

where $r$ is the *coefficient of restitution*.

Equations (4) and (5) represent the mathematical model that we will use for the numerical results using the methods outlined in the next section. It contains five dimensionless parameters, $\alpha$, $\beta$, $\eta$, $r$, and $\hat{\theta}$. In the experimental data the amplitude was set at $\alpha = 0.2258$, which we shall henceforth assume (but see Section 6.2 below), and $\eta$ and $\hat{\theta}$ were used as the main control parameters. That leaves $\beta$ and $r$, both of which contribute to the measured damping ratio $D = 0.07$. Further, a straightforward analysis shows that, in the absence of energy loss at impact,

$$D = \frac{\kappa}{4\omega_0} = \beta. \tag{6}$$

Figure 4(a) shows the result of the numerical solution of (4) and (5) in the freely decaying case ($\alpha = 0$) with $\hat{\theta} = 0$ and $r = 0.7148$ and $\beta = 0.0426$ ($\kappa = 1.1$).

Now it is possible to repeat this numerical experiment for different values of $r$ and $\beta$ and to measure the effective damping $D$ according to the formula (1). In practice, the

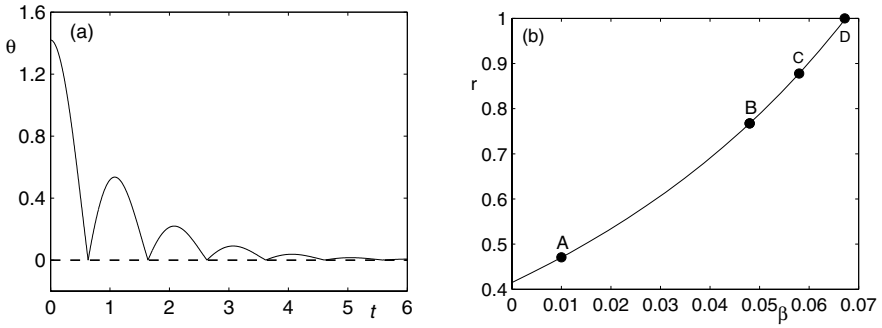


**Fig. 4.** (a) Free decay for an impacting pendulum with no forcing and where the coefficient of restitution $r = 0.7148$ and the damping coefficient $\beta = 0.0426$. (b) The relation between $r$ and $\beta$ to get a damping ratio that is 7% of critical. In (b) the letters A, B, C and D correspond to ($r = 0.4707$, $\beta = 0.01$), ($r = 0.7675$, $\beta = 0.048$), ($r = 0.8778$, $\beta = 0.058$), and ($r = 1$, $\beta = 0.68$), respectively.

value of $D$ was obtained by averaging over several peaks. In so doing, we are able to find a curve in the $(r, \beta)$-plane that corresponds to $D = 0.07$. The result is plotted in Figure 4(b).

We see that when $\beta \approx 0.068$, then $r = 1$, which is unlikely in this experimental set-up, and if no linear damping is assumed ($\beta = 0$), then the estimation of $r$ is close to 0.42. A realistic choice of $r$ for steel on steel contact lies somewhere between 0.5 and 0.8 (see for example [39], [32]), which corresponds to a linear damping coefficient $\beta$ between 0.015 and 0.05. There would then appear to be a degree of freedom in choice of parameters in order to replicate the experimental set-up. This was removed by a simple fitting procedure applied to the numerical replication of the experimental numerical results in Figure 2(d) for $\hat{\theta} = 40^\circ$, by ensuring that the primary grazing bifurcation happens for approximately the observed value of $\eta$ ($\approx 0.445$). This results in the values of $r = 0.7675$ and $\beta = 0.048$ (corresponding to $\kappa \approx 1.238$), marked as point $B$ on the curve in Figure 4(b). Also marked are other values used for comparison in Section 6 below.

## 4. Numerical Methods

We first discuss how to embed the impacting system within a numerical simulation framework, and then how to perform numerical path-following on the nonimpacting orbits.

### *4.1. Simulation*

Consider first the free motion between impacts (4). This can of course be rewritten as the system

$$x' = \begin{pmatrix} x_1' \\ x_2' \\ x_3' \end{pmatrix} = \begin{pmatrix} x_2 \\ \alpha \cos(x_1 + \hat{\theta}) \sin(x_3) - \frac{2\beta}{\eta} x_2 - \frac{1}{4\eta^2} \sin(x_1 + \hat{\theta}) \\ 1 \end{pmatrix} := f(x), \tag{7}$$

where $x_1 = \theta - \hat{\theta}$, $x_2 = \theta'$, and $x_3 = \tau \mod 2\pi$. This definition of $x_3$ causes a jump in the state every time $x_3 = 2\pi$, but this discontinuity can be treated in the same way as the discontinuous jump, at impact, which we shall shortly discuss.

Since it is generally impossible to find explicit solutions to dynamical systems, it is convenient to introduce the flow function $\Phi$ such that $\Phi(x_0, t - t_0)$ corresponds to the point at time $t$ on the trajectory that passes through $x_0$ at time $t_0$. Let $\Phi_t$ denote $\frac{\partial}{\partial t}\Phi$, then in terms of the flow function a general dynamical system (including (7)) can be written as

$$\Phi_t(x, t - t_0) = f(\Phi(x, t - t_0)), \quad \Phi(x, 0) = x_0, \tag{8}$$

for all $x$ and $t$, and the unique solution to (7) is given by $x(t) = \Phi(x_0, t - t_0)$.

In order to implement impact detection, we introduce the function

$$h_{\text{im}}(\theta(t)) = \theta - \hat{\theta} \equiv h(x) = x_1.$$

In practice then, time, angle, and angular velocity of the pendulum at impact is found by monitoring $h_{\text{im}}(x(t))$ during the integration of (7), and when $h_{\text{im}} = 0$, the impact law (5) is applied. Thus effective simulation of the combined hybrid system can occur. In the results that follow, this is implemented in MATLAB using `ode45` with accurate hit-crossing to detect zeros of $h_{\text{im}}$.

### *4.2. Continuation and Stability of Periodic Orbits*

In order to apply the normal form theory that follows, we need to accurately detect periodic solutions and perform continuation of them up to a grazing bifurcation, at which point we also need the linearisation around the periodic orbit. In fact, we derive a more general method for continuation of periodic solutions to hybrid systems of the form

$$\dot{x} = f(x), \qquad h(x) > 0, \tag{9}$$

where $x \in \mathbb{R}^n$ is the state, subject to the impact law

$$x(t_{\text{im}}^+) \leftarrow g(x(t_{\text{im}}^-)), \quad h(x) = 0. \tag{10}$$

By definition, for a periodic orbit, it is possible to find at least one $x^*$ on the orbit such that

$$x^* = \Phi(x^*, T) := \Psi(x^*, T), \tag{11}$$

where $T > 0$ is the period (cf. Figure 5 (a)). Consider a periodic orbit that impacts just once per period. Then, from (11) there exists a time $t_{\text{im}}$, such that $h(\Phi(x^*, t_{\text{im}})) = 0$ and

$$x^* = \Phi_2(g(\Phi_1(x^*, t_{\text{im}})), T - t_{\text{im}}) := \Psi(x^*, T), \tag{12}$$

where $\Phi_1$ and $\Phi_2$ are the flow functions before and after the interaction with $h = 0$, respectively (cf. Figure 5 (c)). Since our focus is on periodic orbits with at most one impact per period and for which only one flow rule applies, we have $\Phi_1 = \Phi_2 = \Phi$.

To locate periodic motions, i.e., to solve eqs. (11) or (12), we will use Newton's method. This method requires the calculation of the flow Jacobian $\Psi_x(x^*, T)$ over one period including discontinuous jumps. Following [33], [1], [43], [10], the Jacobian for a periodic orbit with a single impact is

$$\Psi_x(x^*, T) = \Phi_{2,x}(g(x_{\text{im}}), T - t_{\text{im}})G(x_{\text{im}})\Phi_{1,x}(x^*, t_{\text{im}}), \tag{13}$$

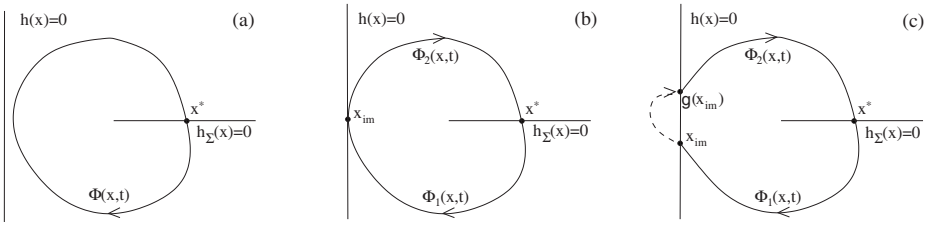


**Fig. 5.** Periodic orbits with (a) no impacts, (b) grazing, and (c) impact once a period.

where the two Jacobians $\Phi_{1,x}$ and $\Phi_{2,x}$ are solutions to the first variational equations before and after the impact and

$$G(x_{\text{im}}) = g_x(x_{\text{im}}) + \frac{f(g(x_{\text{im}})) - g_x(x_{\text{im}})f(x_{\text{im}})}{h_x(x_{\text{im}})f(x_{\text{im}})}h_x(x_{\text{im}}), \tag{14}$$

where $h_x$ and $g_x$ are derivatives of the functions $h$ and $g$ with respect to the state $x$, respectively, and where

$$h_x(x_{\text{im}})f(x_{\text{im}}) \neq 0.$$

The function $G(x_{\text{im}})$ can be derived by using a zero-time discontinuity mapping approach (see [19], [10] and Section 5) and takes into account both changes in the state and vector field before and after the discontinuous jump. This matrix is sometimes referred to as the saltation matrix [31]. Also, since both equations (11) (nonimpacting) and (12) (impacting) consist of $n$ equations for the unknowns, we need to add an extra equation to find a unique periodic solution. A natural choice is a function $h_\Sigma(x) = 0$ that defines a Poincaré surface $\Sigma$. Thus, the equations we want to be fulfilled for a periodic orbit are

$$\Psi(x^*, T) = x^* \qquad \text{and} \qquad h_\Sigma(x^*) = 0. \tag{15}$$

By using (13)–(15), Newton's method can be formulated as

$$\begin{pmatrix} x_{k+1} \\ T_{k+1} \end{pmatrix} = \begin{pmatrix} x_k \\ T_k \end{pmatrix} - \begin{pmatrix} \Psi_x(x_k, T_k) - I & \Psi_t(x_k, T_k) \\ h_{\Sigma,x}(x_k) & 0 \end{pmatrix}^{-1} \begin{pmatrix} \Psi(x_k, T_k) - x_k \\ h_\Sigma(x_k) \end{pmatrix}, \tag{16}$$

where $\Psi_t(x_k, T_k) = f(x_k)$ is the vector field on the surface $\Sigma$ at the point $x_k$. When both $\|x_{k+1} - x_k\|$ and $\|T_{k+1} - T_k\|$ are sufficiently small (within a given tolerance), we choose to let $x^* = x_{k+1}$ be the periodic point on the surface $\Sigma$ and $T = T_{k+1}$ its period. Whenever a periodic orbit has been located, the linear stability of this orbit is given by the Floquet multipliers (i.e., the eigenvalues of the flow Jacobian $\Psi_x(x^*, T)$).

For the parameter continuation of periodic orbits, any path-following method can be used. Specifically we have implemented the pseudo-arclength method (see [27], [29]). The resulting code has been written in MATLAB and can be used to follow an additional constraint in two parameters, such as the condition that grazing occurs at $t_{im}$.

## 5. The Grazing Bifurcation Normal Form

To study grazing motions, we find it convenient to introduce a local transversal Poincaré surface (as in the previous section) through a point on the grazing trajectory that is not on the impacting surface, such that a periodic motion with grazing impacts becomes a fixed point of the Poincaré mapping (cf. Figure 5(b)). Motions with grazing impacts are sensitive to small perturbations, i.e., trajectories starting in a vicinity of the grazing trajectory can experience a low-velocity impact, grazing impact, or no impact at all. Despite this, low-velocity impacts lead to continuous, but nondifferentiable, Poincaré maps. Therefore, following Nordmark and collaborators [35], [34], [36], [19], the low-velocity impacts can be treated separately from the rest of the motion by introducing

so-called *discontinuity maps*. These can be written in the form

$$D(x) = \begin{cases} x + b(x, y)y, & h(x) \le 0, \\ x, & h(x) > 0, \end{cases} \tag{17}$$

where

$$y = \sqrt{-h(x)} \qquad \text{and} \qquad b(x_{\text{im}}, 0) = -\sqrt{2\mathcal{L}_f^2 h(x)}e(x)|_{x=x_{\text{im}}}.$$

For general hybrid dynamical systems of the form (11) subject to an impact law of the form (10), the restitution function $g$ can be written

$$x \leftarrow g(x) = x + e(x)\mathcal{L}_f h(x), \tag{18}$$

where for our system

$$h_x = (1, 0, 0), \qquad \mathcal{L}_f h(x) = h_x f(x) = x_2, \qquad e(x) = (0, -(1 + r), 0)^T,$$

and thus

$$b(x_{\text{im}}, 0) = -\sqrt{2\mathcal{L}_f^2 h(x)}e(x)|_{x=x_{\text{im}}} = -\sqrt{2a(x_{\text{im}})}(0, -(1 + r), 0)^T, \tag{19}$$

where $a = x_2'$ is given by the second component of the right-hand side of (7) and $x_{\text{im}} = (0, 0, t_{\text{im}})^T$. Finally, from (18), (17), and (19), the Poincaré map for the full orbit is given by

$$\Pi(x, T) = \Phi_2(D(\Phi_1(x, t_{\text{im}})), T - t_{\text{im}}), \tag{20}$$

where $T > 0$ is the period of the grazing periodic orbit and $t_{\text{im}}$ is the time ($0 < t_{\text{im}} < T$) when the grazing impact occurs.

We are now in a position to use this map to estimate the behaviour of motions near grazing. The estimations will be compared with experimental results and direct numerical simulations.

## 6. Results

In this section we will compare direct numerical simulations with the experimental results shown in Section 2 and the mapping derived in the previous section. Grazing periodic orbits will be continued and the ability to calculate the stability will be used to explain the period-adding cascade shown in the bifurcation diagrams. Furthermore, we will discuss parameter dependence and how small parameter variations influence the dynamics in resonant regions.

### *6.1. Numerical Results*

Let us first take a look at nonimpacting motion, which is the key to revealing what happens in systems including low-velocity impacts. Figure 6 shows variation in the maximum amplitude of the stable period-one nonimpacting motion for the four different values of

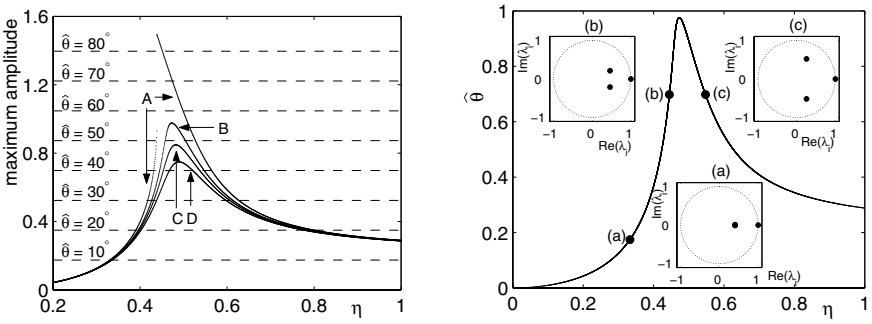


**Fig. 6.** Left: Long-time behaviour of the nonimpacting pendulum for four different damping parameters $\beta$. The letters A, B, C, and D correspond to $\beta = 0.010$, $\beta = 0.048$, $\beta = 0.058$, and $\beta = 0.068$, respectively. Right: Two-parameter (in $\eta$ and $\hat{\theta}$) continuation of grazing periodic orbits where $r = 0.7675$ and $\beta = 0.048$. The corresponding Floquet multipliers $\lambda_i$ are shown in the insets for (a) $\hat{\theta} = 10^\circ$, $\eta = 0.3229$, (b) $\hat{\theta} = 40^\circ$, $\eta = 0.4450$, and (c) $\hat{\theta} = 40^\circ$, $\eta = 0.5475$. The values of the Floquet multipliers are (a) $(1, 0.4040 \pm 0.0114\text{i})$, (b) $(1, 0.4606 \pm 0.2137\text{i})$, and (c) $(1, 0.2534 \pm 0.5178\text{i})$.

the damping parameter illustrated in Figure 4(b). Note that these response curves are obtainable analytically and show a characteristic fundamental resonance peak close to $\eta = 0.5$. For now, let us focus on case *B* ($\beta = 0.048$), which we obtained by parameter-fitting the $\eta$-value of the first grazing bifurcation for the case $\eta = 0.4$. The values of the varying impact stop angle $\hat{\theta}$ are depicted as horizontal lines in the figure at $10^\circ$ intervals. Hence the $\eta$-values at which the first and second grazing bifurcations (which respectively destroy and create period-one nonimpacting motion) can be read off from the graph as in intersection between the response curve and the appropriate horizontal line. The right panel of Figure 6 shows the same response curve computed by numerical continuation, in which we have also computed the Floquet multipliers of the periodic orbit which are depicted at three points along the curve.

The first thing to note from Figure 6 is that there is an upper bound of $\hat{\theta}_{\max}$ beyond which grazing cannot occur for any value of $\eta$ (about $55^\circ$ for case B). Another thing to note is that for $\hat{\theta} = 10^\circ$ there is no second grazing bifurcation to restore period-one non-impacting motion. Both of these accord with what was observed in the experimental data (although the upper bound of $55^\circ$ is somewhat higher than that observed experimentally).

Next we present the results of numerical simulation of the equations (4), (5), sticking to case B of the damping and restitution coefficients. Figure 7 shows Poincaré section brute-force bifurcation diagrams over the same frequency range and values of $\hat{\theta}$ as in the experimental data.

We see the same broad features of the dynamics upon increasing $\eta$ as was observed in the experiment. For each $\hat{\theta}$ there is a first grazing bifurcation that leads to a rapid change in the dynamics, from nonimpacting period-one periodic motion to impacting chaotic motion containing windows of stable periodic orbits in a period-adding cascade. The period is decreased by one for each periodic window as $\eta$ is increased (a reverse period-adding cascade). As in the experimental results, the period of the first appreciable

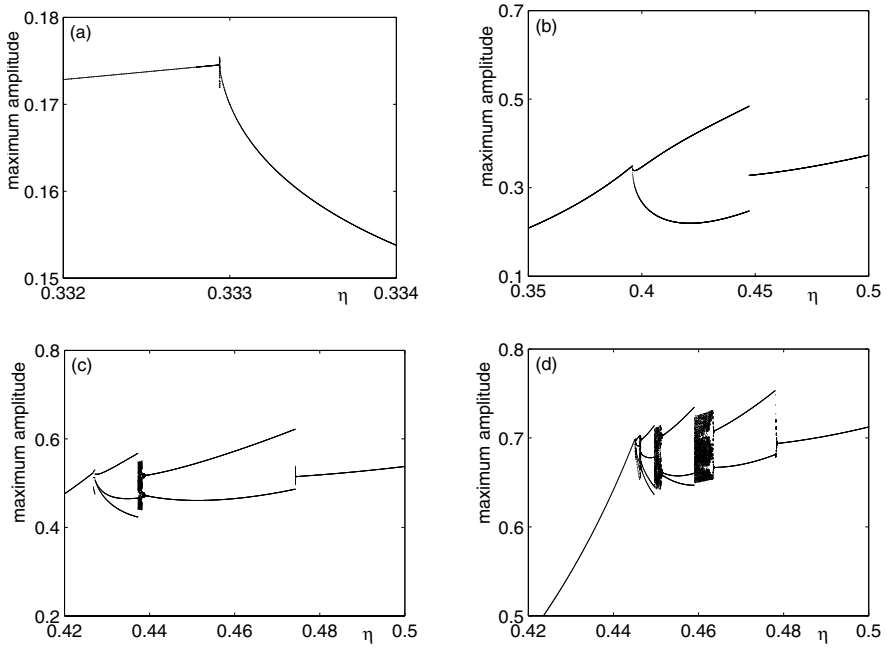


**Fig. 7.** Changes in existence and stability of the forced impacting pendulum under variation of $\eta$ and where (a) $\hat{\theta} = 10^\circ$, (b) $\hat{\theta} = 20^\circ$, (c) $\hat{\theta} = 30^\circ$, and (d) $\hat{\theta} = 40^\circ$, using direct numerical simulation. The coefficient of restitution $r = 0.7675$, the damping coefficient $\beta = 0.048$, and the forcing amplitude $\alpha = 0.2254$.

periodic window is increasing with increasing $\hat{\theta}$, for a specific $\eta$; in this case period-one for $10^\circ$, two for $20^\circ$, three for $30^\circ$, and four (actually, briefly, five) for $40^\circ$.

The period-adding cascade is clearly highlighted in Figure 8(a), which was calculated similarly to Figure 7, but here $\eta$ is held fixed at 0.447 while $\hat{\theta}$ is varied. We now observe a grazing bifurcation at $\hat{\theta} = 41^\circ$ as the onset of a period-adding cascade, where the period increases with $\hat{\theta}$.

Returning to Figure 7, notice that for all cases with $\hat{\theta} > 10^\circ$ the region of impacting behaviour ends with another grazing bifurcation, which results in the destruction of a period-two orbit, just as in the experimental data.

In Figures 9(a) and 9(b) numerical time series are shown for two different cases, ($\hat{\theta} = 10^\circ, \eta = 0.33294$) and ($\hat{\theta} = 40^\circ, \eta = 0.446$), respectively, which qualitatively correspond to the experimental time series shown in Figure 3(a) and 3(c). On the one hand, the numerical and experimental results have similar amplitude, but on the other hand there are some differences in the dynamical characteristics between the numerical and experimental results. These differences have their origins in the differences in the bifurcation diagrams at the particular $\eta$-values given above. As an example, in Figure 3(d) the experiment shows a period-five motion but the numerics show a chaotic motion for the same $\eta$-value, which can be seen in the corresponding bifurcation diagram in Figure 7(d).

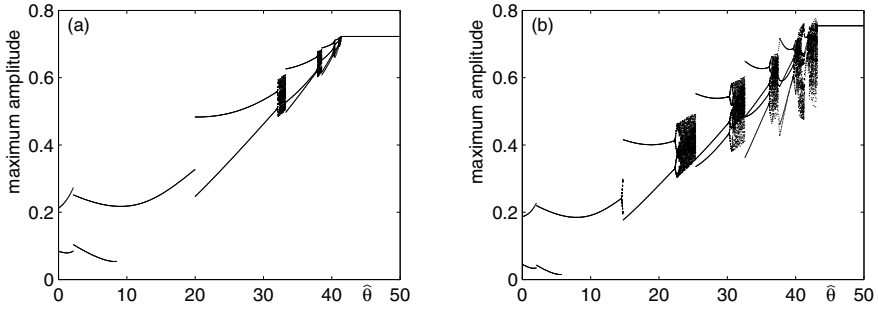


**Fig. 8.** Bifurcation diagrams of the forced impacting pendulum under impact barrier angle $\hat{\theta}$ variation where $\eta = 0.447$. In (a) $r = 0.7675$, $\beta = 0.048$ and in (b) $r = 0.4707$, $\beta = 0.01$. The figures (a) and (b) correspond to case B and case A in the right panel of Figure 6, respectively.

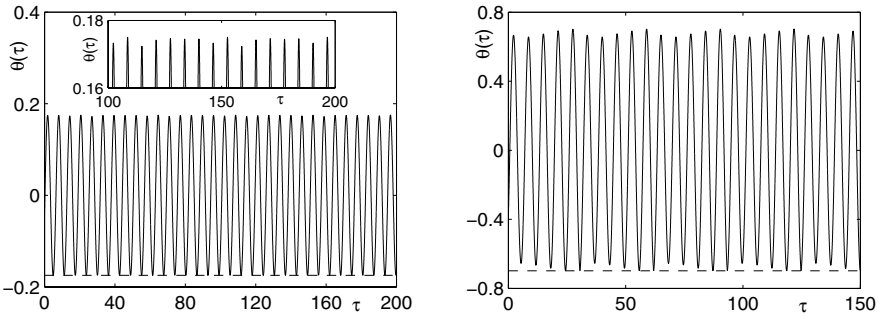


(a) (b)

**Fig. 9.** Sample numerical time series corresponding to the experimental shown in Figure 3, where (a) $\hat{\theta} = 10^\circ$, $\eta = 0.33294$, and (b) $\hat{\theta} = 40^\circ$, $\eta = 0.446$. In (a) the motion is chaotic and in (b) period-5. The inset in (a) is a magnification of the upper part of the time series and visualizes the chaotic motion.

However, if $\eta$ is slightly changed (from 0.45 to 0.446), the numerical simulation gives the same motion characteristics (period-five motion) as the experiment.

Next we will examine how well the Poincaré map $\Pi$, given by (20), derived in Section 5 predicts the dynamics caused by the first grazing bifurcation. The main ingredient required to compute this map is the computation of the linearisation around the grazing periodic orbit. This can be obtained for free from the Jacobian matrix if the periodic orbit is continued using the methods discussed in Section 4.2. The results of a two-parameter continuation (in $\hat{\theta}$ and $\eta$), of the grazing period-one orbit were already shown in the right panel of Figure 6, together with the corresponding Floquet multipliers. We note that one multiplier is always identical to unity, as it should be, and the other two lie within the unit circle, indicating that the orbits are stable. For most parameter values of interest, these two nontrivial multipliers are complex.

Let us focus on the first grazing bifurcation for $\hat{\theta} = 40^\circ$, at $\eta = 0.445$, for which the magnitude of the (largest in magnitude) nontrivial multiplier is $|\lambda| = 0.5114$ (see inset

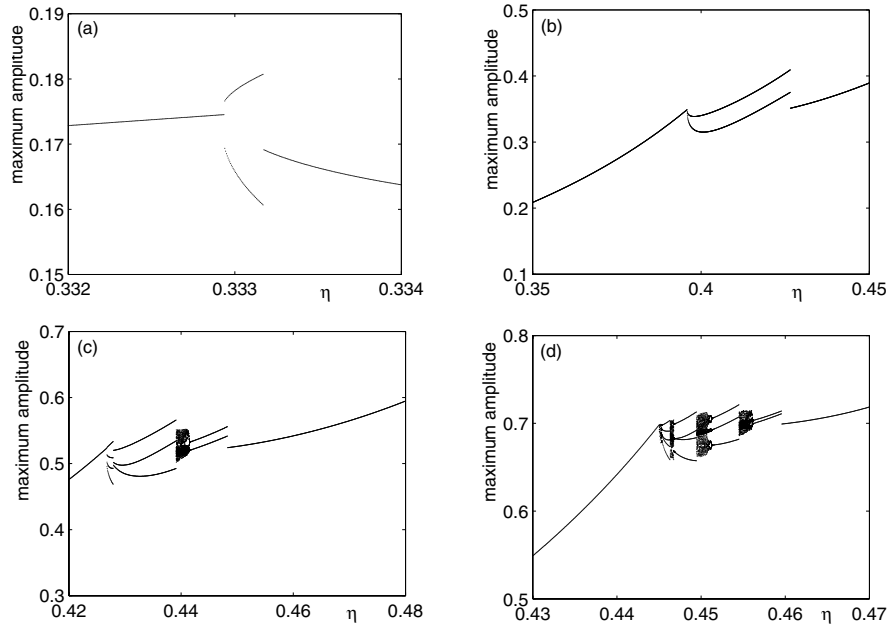


**Fig. 10.** The same results as in Figure 7 but computed using the discontinuity mapping. (a) $\hat{\theta} = 10^\circ$, (b) $\hat{\theta} = 20^\circ$, (c) $\hat{\theta} = 30^\circ$, (d) $\hat{\theta} = 40^\circ$.

(b) of Figure 6). Now, grazing bifurcation theory [8], [18], [37] predicts that if

$$\frac{1}{4} < |\lambda| < \frac{2}{3}, \tag{21}$$

then the bifurcation will cause the onset of a period-adding cascade, which is exactly what we see in Figure 7(d).

Figures 10(a)–(d) use the local discontinuity mapping approach to recreate the bifurcation diagrams in Figure 7. Even though the discontinuity mapping approach is local, the qualitative agreement between the two different methods is good even for $\eta$-values relatively far away from the point of grazing. For instance, the period-adding cascades are captured and clearly visible in Figures 10(c) and (d), but the intervals in which they appear are somewhat shortened.

To further highlight how grazing and low-velocity impact influence the overall dynamics, we can use the map $\Pi$ to compute the shape of the chaotic attractor. Figure 11(b) shows a delay plot (two consecutive iterates of the map; $\theta_{k+1}$ against $\theta_k$) for $\hat{\theta} = 40^\circ$ and $\eta = 0.4458$, i.e., just beyond the first grazing bifurcation. Figure 11(a) shows the same information computed by direct numerical simulation of the equations (4) and (5) using the Poincaré section $\{x_3 := \tau = 0\}$. The agreement between the two is plain to see. For both, the characteristic fingered appearance of the attractor is clearly visible. The almost vertical branches on the left-hand side causes the stretching in the state space (and the chaotic dynamics) and can be explained by the square-root term in the local map for grazing impacts, as discussed in Section 5. The appearance of a number

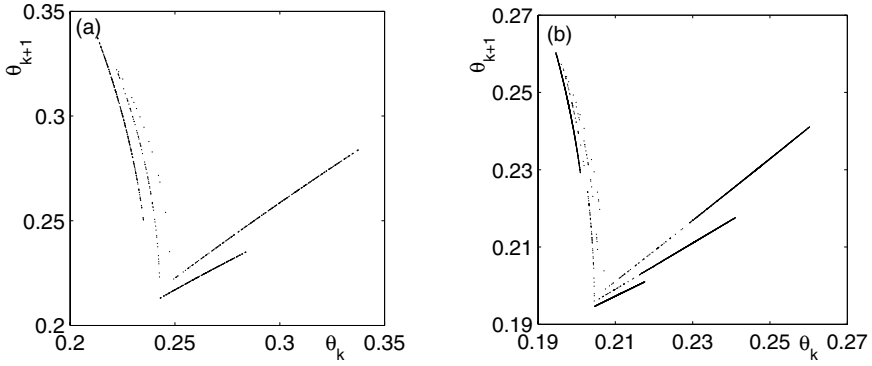


**Fig. 11.** Delay plots for the impacting pendulum near grazing using (a) direct numerical simulation and (b) discontinuity map at Poincaré section $h(x) = x_3 = 0$. In both cases $r = 0.7675$, $\beta = 0.048$, $\eta = 0.4458$.

of parallel branches in the delay plot indicates that the global Poincaré map $\Psi$ is not one-dimensional, which we know to be true.

Finally, consider the reverse grazing bifurcation that occurs for $\eta = 0.5475$ when $\hat{\theta} = 40^\circ$. Here the magnitude of the nontrivial Floquet multipliers satisfies $|\lambda| = 0.5765$ (see inset (c) of Figure 6). Note that, compared with the first grazing bifurcation, this is closer to the upper threshold in (21) for the existence of period-adding cascades according to the theory of grazing bifurcations. This goes some way to explain why the transition back to nonimpacting behaviour is much more sudden and does not appear to involve any appreciable chaotic behaviour.

### *6.2. Parameter Uncertainty*

Looking at Figure 6, we note just how sensitive the height of the resonance peak is to the value of the damping parameter. This has strong implications for the location of the first grazing bifurcation, and indeed for the value $\hat{\theta}_{\max}$ beyond which grazing cannot occur. This also implies that the linearisation around the grazing periodic orbits is highly sensitive to damping, which can cause gross changes in the details of the period-adding cascade close to the grazing point.

To test this sensitivity, we have varied the parameters $\beta$ and $r$ along the curve in Figure 4(b) and found no significant difference in the qualitative picture of the bifurcation diagrams, but large quantitative differences. Figures 8(a) and (b) compare bifurcation diagrams, where the impact barrier angles are varied for fixed $\eta = 0.447$, in damping cases B and A from Figure 4(b), respectively. Both show period-adding cascades, but the case with smaller $\beta$ has significantly wider intervals of chaos and also wider, more appreciable windows of the higher-period periodic windows. These latter results would appear to echo what is observed in the experimental data. Nevertheless, we have not been able to find a single point on the $(r, \beta)$ curve that gives a perfect fit between the numerical and experimental results. In particular, although there is better agreement with the experimental data using case A than case B, this greatly overestimates the value

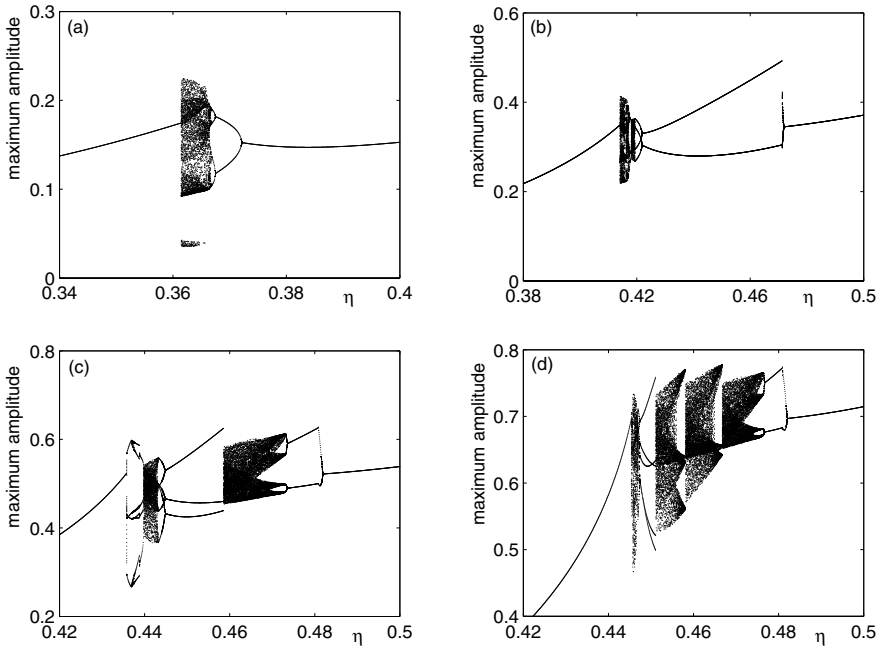


**Fig. 12.** Changes in existence and stability of the forced impacting pendulum under variation of $\eta$ and where $\hat{\theta} = 10^\circ$ (a), $\hat{\theta} = 20^\circ$ (b), $\hat{\theta} = 30^\circ$ (c), and $\hat{\theta} = 40^\circ$ (d). The driving frequency is $0.71\alpha$, the coefficient of restitution $r = 0.4707$, and the damping coefficient $\beta = 0.01$.

of $\hat{\theta}_{\max}$ observed experimentally (recall that no impacting behaviour was observed for $\hat{\theta} = 50^\circ$). There might be a number of reasons for this other than uncertainty in the damping and restitution parameters, such as vibrations in the experimental set-up, errors in the parameter measurements, or wrong assumptions in the mathematical modeling (for example, damping may enter through a nonlinear velocity-dependent term due to coulomb friction in the pivot).

To highlight this uncertainty, we have performed numerical experiments with a lower value of forcing amplitude $0.71\alpha$, keeping the coefficient of restitution $r = 0.4707$ and the damping coefficient $\beta = 0.01$ fixed (case A). One can argue that this is effectively similar to increasing the overall damping in the structure, since both have the effect of lowering the amplitude of the resonance peak. The resulting bifurcation diagrams under $\eta$ variation for $\hat{\theta} = 10^\circ, 20^\circ, 30^\circ, 40^\circ$ are shown in Figures 12(a)–(d), respectively. If we now compare these results with the experimental bifurcation diagrams in Figures 2(a)–(d), the match is a lot better than what was seen in Figures 7(a)–(d). With this perturbed amplitude and with $\hat{\theta} = 10^\circ$(a), $30^\circ$(c), $40^\circ$(d), the bifurcation diagrams are uncannily similar to those observed in the experiments, and even in the other two cases, we can clearly see one large periodic window surrounded by chaotic regions, culminating in a period-two window.

## 7. Discussion

This paper has sought to use the experimental data from an experiment on a one-degree-of-freedom impacting pendulum in order to justify the approach that has become standard in the study of grazing bifurcations, namely, to derive the square-root normal-form map using Nordmark's idea of the discontinuity mapping. These days, one has come to expect chaotic dynamics in forced pendulum systems, but perhaps the most striking feature of the experimental results are the sudden abrupt jump to chaos and the cascade of period windows whose period increases by one cycle in subsequent windows (a so-called period-adding cascade). This is precisely the dynamics that the grazing bifurcation normal form predicts. Moreover we have attempted a quantitative explanation of the experimental observations, via direct numerical simulations, periodic-orbit continuations methods, and careful construction of the discontinuity mappings. One side result has been to show just how good a match can be found between the discontinuity mapping approach and the direct numerical simulation. In seeking a match with the experimental data, we have indeed found that the normal form is precisely in the right region for period-adding and chaos to occur, but a precise quantitative fit is more troublesome (these conclusions echo those in a similar study [20], in which impacts of a pipe conveying fluid are analyzed experimentally and numerically).

Our results have highlighted the crucial role played by damping in organizing the finer features of the observed dynamics. Of course, the coefficient of restitution associated with impact causes damping of the impacting behaviour. So, in previous studies that have considered experimental comparison with dynamics that always impacts (e.g. [39]), it was not so crucial whether damping is taken account of via restitution or a linear viscous term. However, in this study we have been interested in precisely the transition between nonimpacting and impacting behaviour, and so both viscous and restitution damping play a crucial role. As the final results produced in the previous section show (see Figure 12), the key to obtaining close quantitative agreement with the experiments is to get the correct amplitude of the pre-impacting orbit, which in this case was obtained by adjusting the forcing amplitude from its true value. As already intimated, this effective amplitude adjustment may be due to the damping occurring via effects that we have not modelled, such as nonlinear coulomb friction or structural interactions.

This paper also shows the importance of careful parameter value estimations when trying to explain experimental results using a mathematical model, especially ones that exhibit the infinite local stretching inherent in the square-root map. Often one can use simplified models with a few essential parameters, but it is also likely that the original real-world system has a large number of significant parameters that cannot easily be simplified or ignored. Even worse, some of the parameters can have a stochastic behaviour (due to noise from various sources) which requires analysis using methods that go beyond this paper.

## Acknowledgments

This work was supported by the EU FP5 Project SICONOS (Grant no. IST-2001-37172). A. Nordmark is acknowledged for sharing his insights into grazing bifurcations.

## References


[1] J. Adolfsson, H. Dankowicz, and A. Nordmark. 3D passive walkers: Finding periodic gaits in the presence of discontinuities. *Nonlin. Dynam.*, 24:205–229, 2001.

[2] M. A. Aizerman and E. S. Pyatnitskii. Foundations of a theory of discontinuous systems. I–II. *Automation and Remote Control* 35(7):1066–1079, 1242–1262, 1974.

[3] V. I. Babitskii. *Theory of Vibroimpact Systems: Approximate methods*. Nauka, Moscow, 1978.

[4] P. V. Bayly and L. N. Virgin. An experimental study of an impacting pendulum. *J. Sound Vib.*, 164(2):364–374, 1993.

[5] B. Brogliato. *Nonsmooth Mechanics: Models, Dynamics and Control*. Springer-Verlag, New York, 1999.

[6] C. J. Budd and F. Dux. Chattering and related behaviour in impact oscillators. *Phil. Trans. Roy. Soc. Lond. A*, 347:365–389, 1994.

[7] D. R. J. Chillingworth. Discontinuity geometry for an impact oscillator. *Dynam. Syst.*, 17:380–420, 2002.

[8] W. Chin, E. Ott, H. E. Nusse, and C. Grebogi. Grazing bifurcations in impact oscillators. *Phys. Rev. E*, 50:4427–4444, 1994.

[9] H. Dankowicz and A. B. Nordmark. On the origin and bifurcations of stick-slip oscillations. *Physica D*, 136:280–302, 1999.

[10] H. Dankowicz and P. T. Piiroinen. Exploiting discontinuities for stabilization of recurrent motions. *Dynam. Syst.*, 17:317–342, 2002.

[11] J. H. B. Deane and D. C. Hamill. Analysis, simulation and experimental study of chaos in the buck concerter. In *Proceedings of the Power Electronics Specialists Conf. (PESC 1990)*, pp. 491–8, IEEE Press, New York, 1990.

[12] R. L. Devaney. *An Introduction to Chaotic Dynamical Systems*. Addison-Wesley, Reading, Mass., 2nd ed., 1989.

[13] M. di Bernardo, C. J. Budd, and A. R. Champneys. Corner-collision implies border-collision bifurcation. *Physica D*, 154:175–194, 2001.

[14] M. di Bernardo, M. I. Feigin, S. J. Hogan, and M. E. Homer. Local analysis of C-bifurcations in $n$-dimensional piecewise smooth dynamical systems. *Chaos, Solitons and Fractals*, 10:1881–1908, 1999.

[15] M. di Bernardo, P. Kowalczyk, and A. Nordmark. Bifurcations of dynamical systems with sliding: Derivation of normal-form mappings. *Physica D*, 170:175–205, 2002.

[16] M. I. Feigin. Doubling of the oscillation period with $C$-bifurcations in piecewise continuous systems. *PMM*, 34:861–869, 1970. In Russian.

[17] M. I. Feigin. *Forced Oscillations in Systems with Discontinuous Nonlinearities*. Nauka, Moscow, 1994. In Russian.

[18] M. H. Frederiksson and A. B. Nordmark. Bifurcations caused by grazing incidence in many degrees of freedom impact oscillators. *Proc. Roy. Soc. Lond. A*, 453:1261–1276, 1997.

[19] M. H. Frederiksson and A. B. Nordmark. On normal form calculations in impact oscillators. *Proc. Roy. Soc. Lond. A*, 456:315–329, 2000.

[20] M. H. Fredriksson, D. Borglund, and A. B. Nordmark. Experiments on the onset of impacting motion using a pipe conveying fluid. *Nonlin. Dynam.*, 19:261–271, 1999.

[21] H. Goyder and C. Teh. A study of the impact dynamics of loosely supported heat exchanger tubes. *J. Pressure Vessel Tech.*, 111:394–401, 1989.

[22] J. Guckenheimer and P. Holmes. *Nonlinear Oscillations, Dynamical Systems, and Bifurcations of Vector Fields*. Applied Mathematical Sciences, vol. 42. Springer-Verlag, New York, 1983.

[23] N. A. Halliwell, A. D. Batako, and V. I. Babitsky. A self-excited system for percussive-rotary drilling. *J. Sound Vib.* 259(1):97–118, 2003.
[24] J. Jerrelind and A. Stensson. Braille printer dynamics. In *Proceedings of 1999 ASME Design Engineering Technical Conferences*, 1999.
[25] J. Jerrelind and A. Stensson. Nonlinear dynamic behaviour of coupled suspension systems. *Meccanica*, 38:43–59, 2003.
[26] A. Kaharaman and R. Singh. Nonlinear dynamics of a spur gear pair. *J. Sound Vib.*, 142:49–75, 1990.
[27] H. B. Keller. *Lectures on Numerical Methods in Bifurcation Problems*. Springer-Verlag, New York, 1987.
[28] A. M. Krivtsov and M. Wiercigroch. Dry friction model of percussive drilling. *Meccanica*, 34, 1999.
[29] Yu. A. Kuznetsov. *Elements of Applied Bifurcation Theory*. Applied Mathematical Sciences, vol. 112. Springer-Verlag, New York, 2nd ed., 1998.
[30] Yu. A. Kuznetsov, S. Rinaldi, and A. Gragnani. One-parameter bifurcations in planar fillipov systems. *Int. J. Bifurcation & Chaos*, 13:2157–2188, 2003.
[31] R. Leine. *Bifurcations in Discontinuous Mechanical Systems of Filippov-Type*. Ph.D. thesis, Teknische Universiteit Eindhoven, The Netherlands, 2000.
[32] J. L. Meriam and L. G. Kraige. *Engineering Mechanics: Dynamics*, vol. 2. Wiley, New York, 5th ed., 2003.
[33] P. C. Müller. Calculations of Lyapunov exponents for dynamical systems with discontinuities. *Chaos, Solitons and Fractals*, 5:1671–1681, 1995.
[34] A. Nordmark. *Grazing conditions and chaos in impacting systems*. Ph.D. thesis, Royal Institute of Technology, Stockholm, Sweden, 1992.
[35] A. B. Nordmark. Nonperiodic motion caused by grazing incidence in an impact oscillator. *J. Sound Vib.*, 145(2):279–297, 1991.
[36] A. B. Nordmark. Universal limit mapping in grazing bifurcations. *Phys. Rev. E*, 55:266–270, 1997.
[37] A. B. Nordmark. Existence of periodic orbits in grazing bifurcations of impacting mechanical oscillators. *Nonlinearity*, 14:1517–1542, 2001.
[38] H. Nusse, E. Ott, and J. Yorke. Border collision bifurcations: An explanation for observed bifurcation phenomena. *Phys. Rev. E*, 49:1073–1076, 1994.
[39] M. Oestreich, N. Hinrichs, K. Popp, and C. J. Budd. Analytical and experimental investigation of an impact oscillator. *Proceedings of the ASME 16th Biennial Conf. on Mech. Vibrations and Noise*, DETC97VIB-3907:1–11, 1997.
[40] F. Peterka. Part 1: Theoretical analysis of $n$-multiple $(1/n)$-impact solutions. *CSAV Acta Technica*, 19:462–473, 1974.
[41] F. Peterka. Part 2: Results of analogue computer modelling of the motion. *CSAV Acta Technica*, 19:569–580, 1974.
[42] F. Pfeiffer and C. Glocker. *Multibody dynamics with unilateral constraints*. John Wiley & Sons, New York, 1996.
[43] P. T. Piiroinen and H. J. Dankowicz. Low-cost control of repetetive gait in passive bipedal walkers. To appear in *Int. J. Bifurcation & Chaos*, 2005.
[44] K. Popp and P. Shelter. Stick-slip vibrations and chaos. *Phil. Trans. Roy. Soc. A*, 332(1624):89–105, 1990.
[45] S. W. Shaw and P. J. Holmes. Periodically forced linear oscillator with impacts: Chaos and long-periodic motions. *Phys. Rev. Lett.*, 51:623–626, 1983.
[46] K. N. Slade, L. N. Virgin, and P. V. Bayly. Extracting information from interimpact intervals in a mechanical oscillator. *Phys. Rev. E*, 56(3):3705–3708, 1997.

[47] A. Stensson and A. Nordmark. Experimental investigation of some consequences of low velocity impacts in the chaotic dynamics of a mechanical system. *Phil. Trans. Roy. Soc. Lond. A*, 347:439–448, 1994.
[48] W. J. Stronge. *Impact Mechanics*. CUP, Cambridge, 2000.
[49] J. M. T. Thompson and R. Ghaffari. Chaotic dynamics of an impact oscillator. *Phys. Rev. A*, 27:1741–1743, 1983.
[50] L. N. Virgin. *Introduction to Experimental Nonlinear Dynamics: A Case Study in Mechanical Vibration*. Cambridge University Press, Cambridge, 2000.
[51] D. J. Wagg, G. Karpodinis, and S. R. Bishop. An experimental study of the impulse response of a vibro-impacting cantilever beam. *J. Sound Vib.*, 228:242–264, 1999.
[52] G. S. Whiston. Global dynamics of a vibro-impacting linear oscillator. *J. Sound Vib.*, 118:395–429, 1987.
[53] G. S. Whiston. The vibro-impact response of a harmonically excited and preloaded one-dimensional linear oscillator. *J. Sound Vib.*, 115:303–324, 1987.
[54] G. S. Whiston. Singularities in vibro-impact dynamics. *J. Sound Vib.*, 152:427–460, 1992.
[55] S. R. Reid and G. Zhou, eds. *Impact on Behaviour of Fibre-Reinforced Composite Material and Structure*. Woodhead Publication Ltd., Cambridge, UK, 2000.